Acta Sci. Pol.
Formatio Circumiectus 25 (2) 2026, 95–111
ENVIRONMENTAL PROCESSES

www.acta.urk.edu.pl ISSN 1644-0765 DOI: http://doi.org/10.15576/ASP.FC/221075

ORIGINAL PAPER Accepted: 24.04.2026

A HYBRID APPROACH OF FREQUENCY RATIO MODEL AND GEOSPATIAL TECHNOLOGY FOR LANDSLIDE SUSCEPTIBILITY MAPPING: A CASE STUDY

Vinay Purohit 0000-0002-6373-2183, Kishan Singh Rawat✉ 0000-0001-5900-8195, Akshay Mehta 0009-0002-1596-4200

Geo-Informatics, Department of Civil Engineering, Graphic Era (Deemed to be University) Dehradun, Uttarakhand, India

ABSTRACT

Aim of the study
To generate a landslide susceptibility map using Hybrid Approach of FR Model and Geospatial Technology for the studied area

Material and methods
Application of FR Model and GIS

Results and conclusions
According to the FR method, 11.5% areas are very highly susceptible to landslides, 23.2% represents highly susceptible area, and 26.2% represents moderately susceptible areas. Low susceptibility areas constitute 26.5%, and very low susceptibility areas, 12.6%. Susceptibility classes in the final map were derived from FR method, grouped into five risk levels and examined with the value of area under curve (AUC). When it came to zoning the study regions in relation to past landslides, the FR model produced an AUC of 73.4%. Therefore, using the assessment of the landslide susceptibility map, it has been demonstrated that the approaches employed produced findings that were satisfactory in their reliability.

Keywords: frequency ratio, analytical hierarchical process, landslide susceptibility, GIS, remote sensing

INTRODUCTION

Landslides constitute a major natural hazard, particularly in mountainous regions where they can cause severe losses and damage to roads, buildings, other built structures, property, and human life. The Indian Himalayan Zone, which is substantially susceptible to landslides due to its steep and uneven terrain and climatic conditions, is home to approximately 76 million people (Chouhan and Mukherjee, 2023). These slope movements have shown increasing occurrence in the Himalaya-mountain region over the past decades as a result of both anthropological and natural processes (Dubey et al., 2023). Every rainy season, several landslides and slope instability problems are experienced in the Himalayan highlands (Kirschbaum et al., 2015; Dubey et al., 2023). A landslide incident arises from the combined influence of various geoenvironmental factors and human activities.

The growing landslide occurrence and their increasing intensity require predictive models for haz-

✉e-mail: ksr.kishan@gmail.com

© Copyright by Wydawnictwo Uniwersytetu Rolniczego w Krakowie, Kraków 2026

ard prone areas. Landslide susceptibility mapping (LSM) is a significant tool in this context, offering crucial information for disaster preparedness and risk reduction. Several mass movement assessment models are available that vary in both complexity and scale for hazard probability assessments (Christen et al., 2010; Mergili et al., 2017). Comparable multisensor workflows using combined optical and Cband SAR data, processed in SNAP and GIS, have been demonstrated for highresolution hazard mapping in Assam (Mehta and Rawat, 2023). Physically-based models typically demand a large amount of information, including detailed topography data, soil characteristics, geotechnical assessments, descriptions of the groundwater table, and precipitation data. Acquiring such data at the specific time and at the required spatial resolution levels – especially from remote or isolated regions, such as the Himalaya, range may be challenging. The quality and accuracy of the model outputs could potentially be affected by limited data availability. In landslide susceptibility mapping (LSM), statistical models such as Analytic Hierarchy Process (AHP) and Frequency Ratio (FR) are often applied for rapid assessment of areas prone to landslides. Selection measures for LSM in different regional settings have shown that performance and suitability of AHP and FR are high, and both can be demonstrated as working effectively, although ultimately their viability remains dependent upon conditions related to the particular region (Abedini and Tulabi, 2018). Likewise, the study carried out in Jiangxi Province (China) shows how these models are suitable for landslide risk assessment while insisting on collecting high-resolution spatial data and keeping well-maintained landslide inventories with sufficient quality (Huang et al., 2020).

Bisht et al. (2024) and Youssef et al. (2023) propose landslide risk analysis using applied statistical approaches, including the Frequency Ratio (FR) model supplemented with the Prediction Rate (PR). In this study, landslide susceptibility mapping was carried out in the Tanakpur block of Champawat district (Uttarakhand) using Frequency Ratio method with overlay analysis. Due to the difficult topography and fluctuating climate, this area is very susceptible to landslides. The Frequency Ratio (FR) model is a traditional technique that has been chiefly used in several, specific geographic regions because of its potential to couple various landslide conditioning factors and provide reliable susceptibility estimates.

MATERIAL AND METHODS

Study area

Tanakpur block is in Champawat District, India. The region, which has a total size of 982.224 km^2, is located between latitudes of 28°59′41.916 N and 29°22′49.8 N, and longitudes of 79°53′40.068 E and 80°18′59.41 E (Fig. 1). In the research area, ground elevation values vary between 180 m in the NE and 2194 m in SW and E, with a mean elevation of 571 m.

Apart from being a humid subtropical zone, the region has significant monsoonal interaction, making it highly prone to slope failures due to intense rainfall. Geologically, the area consists of several litho units such as Bhaber Tarai Alluvium, Klippen of Crystalline and Lower Paleozoic Granite, Nagthat Formation, Piedmont Fan Surface and Siwalik Group rocks (Jayangondaperumal et al., 2018).

Land cover in the region is predominantly tree cover, succeeded by grassland and cropland. The combination of steep slopes, fragile lithology, intense precipitation, and anthropogenic disturbances such as road construction and deforestation makes the area highly prone to landslides.

Data collection

The first step of Landslide simulation model (LSM) is to develop a landslide inventory, which is essential to this work. This step is absolutely crucial since the reliability of landslide database used for calibrating model directly affects the reliability of LSM. Therefore, the enhanced reliability and caliber of the landslide record correspondingly enhance the forecasting efficiency of susceptibility maps.

For the Tanakpur block, a detailed landslide inventory has been used by combining object interpretation using (a) historical data, (b) field surveys (Fig. 2), and (c) remote sensing (RS) imagery. The inventory thus collated will form the basis for analyzing the spatial pattern of landslides and their correlation with various determinants. Overall, 251 primary landslides were mapped in the region. All three of these modes of collecting data which are mostly

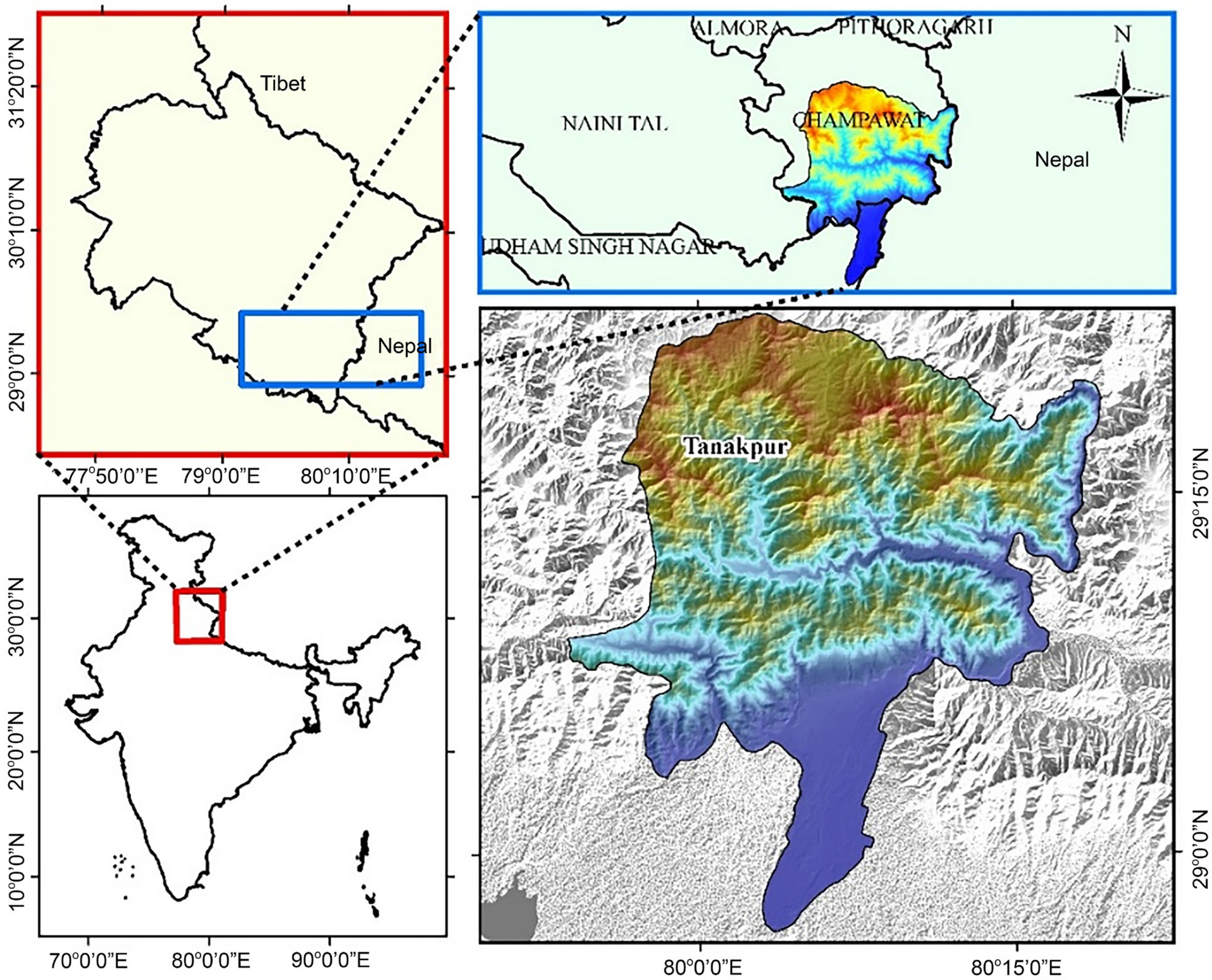

Fig. 1. Study area map of the Tanakpur block, Champawat District, Uttarakhand, India (Source: Authors' own elaboration based on SRTM DEM and administrative boundary data)

related to rock and debris as well as earth flow, are what characterize landslides in the studied region. Out of the 251 landslides found in the region covered by the research, the majority exhibit mostly translational and rotational slides, while the remaining landslides display complicated slides with debris association. The whole area covered by these detections was 3200720.23 m^2.

Thematic data preparation

Total 14 Landslide conditioning factors (LCFs) were found and employed in the simulation of the LS across the study region, based on a thorough assessment of the data and the site's physical attributes. These LCFs include Slope, Curvature, Aspect, Land use and Land cover, Lithology, Rainfall, Soil, Solar radiation intensity over terrain, Earthquake magnitude density, Soil moisture index, Distance to stream, Road, Lineament, and Faults (Figure 3: A–O). In the adjacent Lesser Himalayan region, 72.9% accuracy was achieved in GIS-based landslide susceptibility mapping while considering Slope, Curvature of slope, Aspect, Drainage proximity, Lineament, Density, Lithology and Land use and Land cover (LULC) conditions (Bisht and Rawat, 2024). A multicollinearity among the variables was evaluated, to rule out significant correlations between them. The terrain characteristics were retrieved from DEM-SRTM (Slope, Curvature, Stream, Aspect) with 30 m spatial resolution, ESA world cover V200 (LULC), TRMM (rainfall), Ancillary sources (Soil), Solar radiation (Global Solar Atlas), and Bhukosh (Lithology, Road, Urban, Landslides, Seismicity, Lineament/Faults). Details are given in Table 1 as follows:

Table 1. Conditioning factors and data sources (Source: Authors' own elaboration)

Conditioning factors	Data type/Conversion	Resampled form	Data source/Processing platform
Slope	SRTM-GDEM/ Raster	30 m × 30 m	https://earthexplorer.usgs.gov/
Curvature	SRTM-GDEM/ Raster	30 m × 30 m	
Aspect	SRTM-GDEM/ Raster	30 m × 30 m	
Stream	SRTM-GDEM/ Raster	30 m × 30 m	
Lithology	Bhukosh/Raster	30 m × 30 m	https://geodataindia.gov.in/
Fault	Bhukosh/Raster	30 m × 30 m	https://geodataindia.gov.in/
Lineament	Bhukosh/Raster	30 m × 30 m	https://geodataindia.gov.in/
Earthquake magnitude	Bhukosh/Raster	30 m × 30 m	https://geodataindia.gov.in/
LULC	Esa World cover v200/Raster	30 m × 30 m	https://earthengine.google.com/
Rainfall	CHIRPS-Interpolated/Raster	30 m × 30 m	https://earthengine.google.com/
Soil moisture index	Sentinel-2/Raster	30 m × 30 m	https://earthengine.google.com/
Soil	Ancillary/Raster	30 m × 30 m	literature
Solar radiation	Global Solar Atlas/Raster	30 m × 30 m	https://globalsolaratlas.info/support/data-sources
Road	OSM Layers/Bhuvan	30 m × 30 m	https://bhuvan-app1.nrsc.gov.in/thematic/thematic/index.php

Fig. 2. Field photographs of landslide activities in Tanakpur block (Photo by the authors)

CONDITIONING AND TRIGGERING FACTORS

1. Terrain factors:

Slope – slope gradient is a major determinant in landslide susceptibility analysis, as the likelihood of slope failure is directly correlated with the angle of inclination. As the slope angle increases, so does the probability of mass movement. In this study (Fig. 3A), slope angles were categorized into five distinct classes: very gentle (0–15°), gentle (15–30°), moderately steep (30–45°), very steep (45–60°), and escarpment/cliff (> 60°). The spatial distribution of landslides within these classes revealed that 36.3%, 42.28%, 19.79%, 1.62%, and 0.02% of landslides occurred within the respective slope ranges of 0–15°, 15–30°, 30–45°, 45–60°, and > 60°.

Curvature – curvature of the terrain, particularly profile curvature, quantifies the rate of change in slope gradient and serves as a valuable predictor in landslide risk assessment. Based on a Digital Elevation Model (DEM), the curvature map was distributed into three categories. Curvature (form) was used to describe the concavity and convexity of slopes: negative values mean that slope is concave, and positive values indicate a convex slope (Fig. 3B). The convex and concave area affect the concentration of water flow, thus, resulting in slope saturation and increased failure hazard. In this study, 50.32% of the landslides took place on concave slopes (< 0), 4.25% on flat slopes (0), and 45.43% on convex slopes (> 0).

Aspect – the aspect has a profound impact on the amount of solar radiation received by a slope affecting soil moisture content and, as a consequence, impacting slope stability. The study area was derived a slope aspect map based on the Digital Elevation Model (DEM). The aspect was classified into ten categories: Flat (−1°), North (0–22.5°), Northeast (22.5–67.5°), East (67.5–112.5°), Southeast (112.5–157.5°), South (157.5–202.5°), Southwest (202.5–247.5°), West (247.5–292.5°), Northwest (292.5–337.5°), and North (337.5–360°) (Fig. 3D). The distribution of landslides across these aspect classes revealed that 0.47% occurred on flat surfaces, while 5.77%, 11.82%, 13.73%, 14.92%, 15.21%, 12.19%, 10.66%, 10.08%, and 5.16% of landslides happened on slopes facing North, Northeast, East, Southeast, South, Southwest, West, Northwest, and North, respectively.

2. Geological factors:

Lithology – lithology strongly influences slope stability because different rock types exhibit varying mechanical strength and weathering characteristics. The lithological map was adapted from Thakur and Rawat (1992) to represent geological variability within the study area (Fig. 3F). Six lithological units were identified: Nagthat Formation, Lower Paleozoic Granite, Klippen of Crystalline, Siwalik Group, Piedmont Fan Surface, and Bhaber–Tarai Alluvium.

Fault – faults represent structurally weakened zones that reduce rock mass stability and may facilitate landslides by increasing fracturing, permeability, and pore-water pressure. Distance to fault was calculated using buffer analysis from mapped fault lines (Fig. 3M).

Lineament – lineaments indicate zones of structural weakness such as fractures and minor shear zones that may promote slope instability. Unlike the fault layer, lineaments also include smaller fractures not mapped as major tectonic faults. A Euclidean distance map was generated from the lineament layer and classified into five distance bands (0–500 m, 500–1000 m, 1000–1500 m, 1500–2000 m, and > 2000 m) to evaluate landslide frequency relative to fracture proximity (Fig. 3L).

3. Hydrological and land cover factors:

Stream – proximity to drainage networks influences slope saturation and toe erosion, thereby affecting landslide susceptibility. The drainage network was extracted from SRTM-GDEM data, and distance to drainage was classified into five buffer zones: 0–100 m, 100–200 m, 200–300 m, 300–400 m, and > 400 m (Fig. 3C).

Rainfall – rainfall plays a key role in triggering landslides due to its influence on soil saturation and pore-water pressure. Annual rainfall data for 2023 were obtained from the Climate Hazards Group InfraRed Precipitation with Station Data (CHIRPS) and processed in Google Earth Engine. The rainfall distribution map was generated using inverse distance weighting (IDW) interpolation in GIS (Fig. 3G).

LULC – Sentinel-2 based world cover v200 Landuse and Landcover map was used, classifying Tanakpur block into major physiographic classification with an accuracy of more than 0.8. The figures of GEE were generated from the data processed in Google earth engine (GEE) as depicted in Fig. 3E.

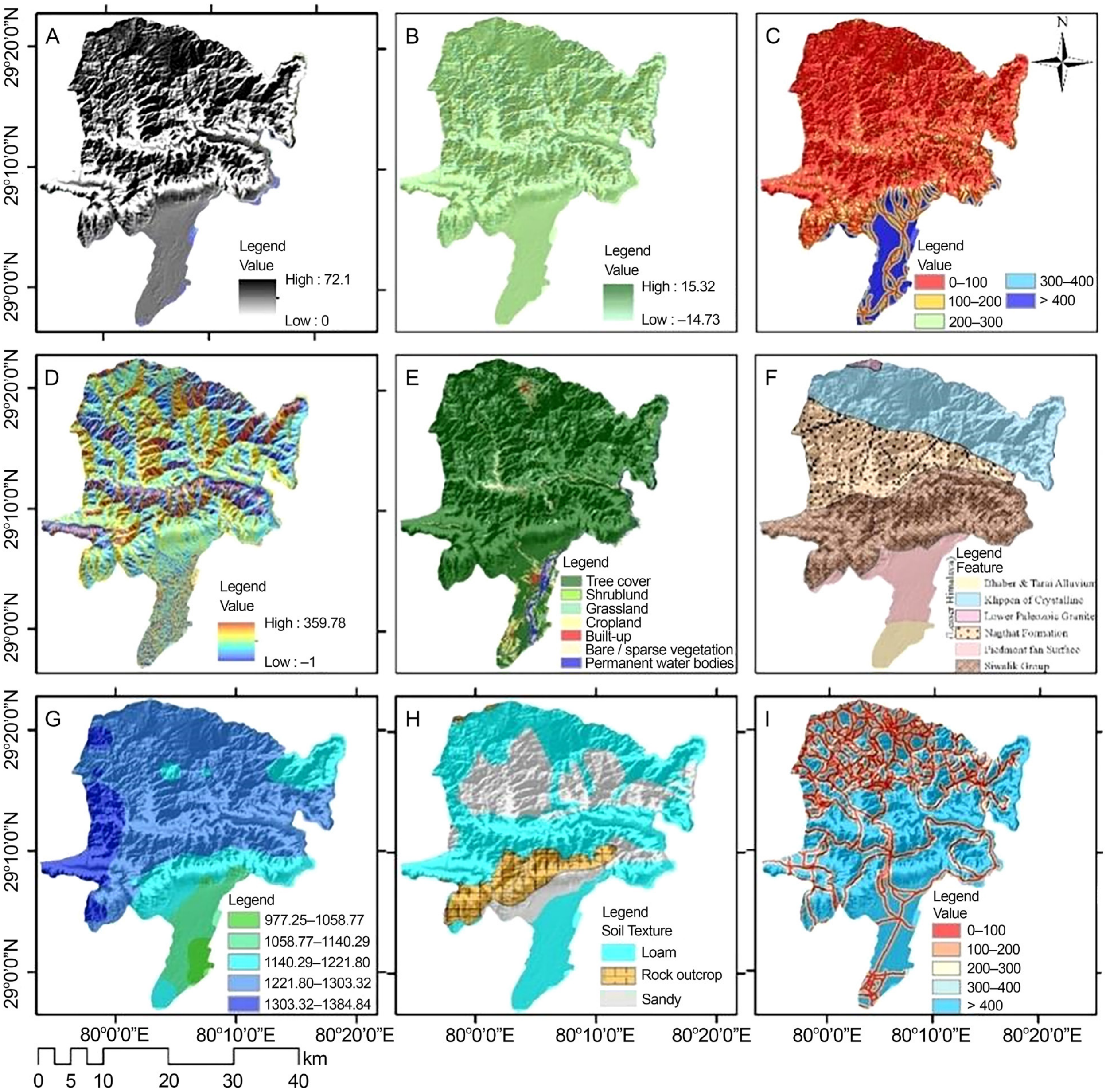

Fig. 3. Landslide conditioning factors (LCFs): (A) Slope; (B) Curvature; (C) Distance to stream; (D) Aspect; (E) Landuse and Landcover; (F) Lithology; (G) Rainfall; (H) Soil; (I) Distance to road; (J) Solar radiation; (K) Earthquake magnitude density; (L) Distance to lineament; (M) Distance to fault; (N) Soil moisture index; (O) Landslide point map of study area (Source: Authors' own elaboration based on SRTM DEM)

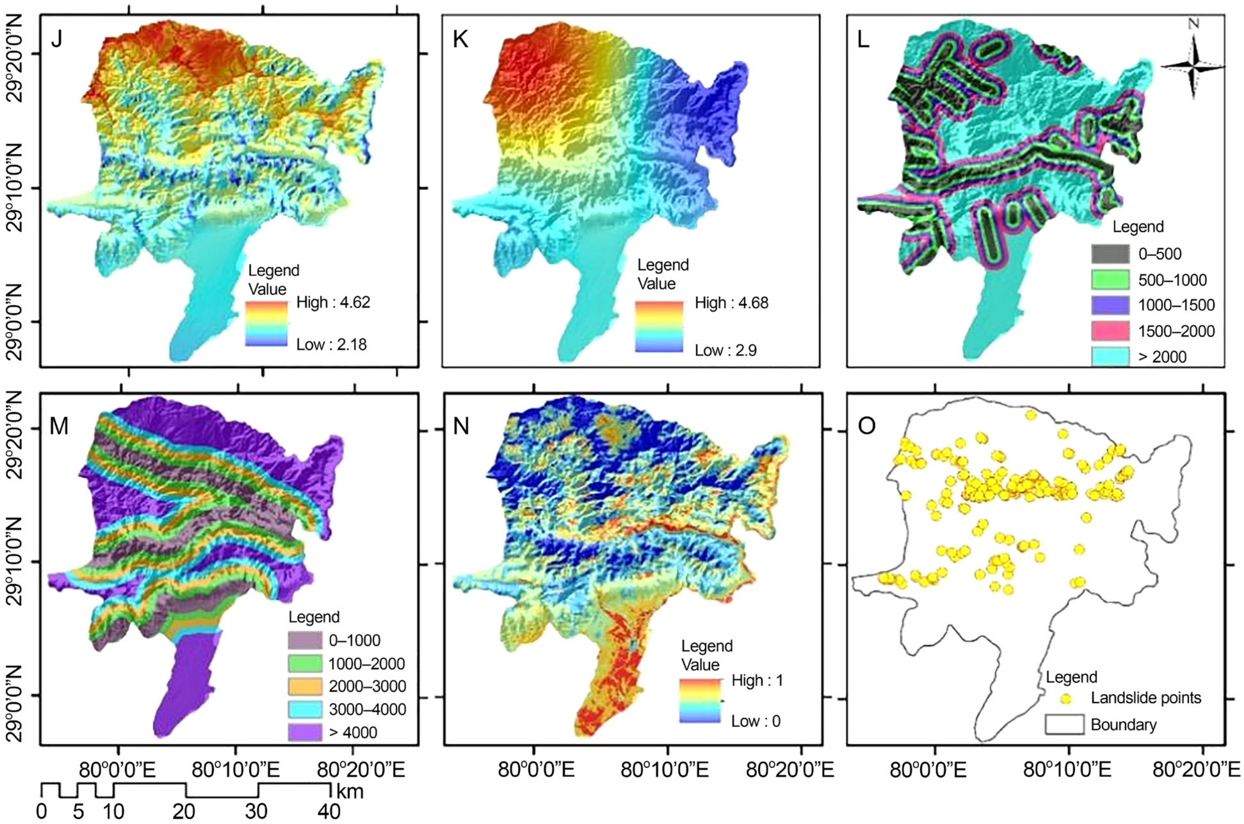

Fig. 3. cont.

Soil – soil properties influence slope stability due to their cohesion, shear strength, and water retention characteristics. Soil type data for the study area were classified into loam, rock outcrop, and sandy soil categories for susceptibility assessment (Fig. 3H).

4. Triggering factors:

Solar radiation – solar radiation influences landslide susceptibility as it impacts soil moisture dynamics and vegetation cover. A solar radiation layer was derived from the DEM to represent spatial variability in insolation across the study area (Fig. 3J).

Earthquake magnitude – seismic activity can trigger landslides by inducing ground shaking and slope destabilization. Earthquake magnitude density was included as a regional seismic trigger indicator to account for the influence of Himalayan tectonic activity on slope instability (Fig. 3K).

Distance to road – road construction and associated cut-and-fill operations may alter slope geometry, drainage, and toe support, thereby affecting slope stability. Distance to road was used as a proxy for anthropogenic disturbance and was calculated using Euclidean distance from the road network. The resulting raster was categorized into five distance bands: 0–100 m, 100–200 m, 200–300 m, 300–400 m, and > 400 m (Fig. 3I).

Soil Moisture Index – the Soil Moisture Index (SMI) was included to represent spatial variation in soil wetness, which influences pore-water pressure and slope stability. Higher soil moisture conditions are associated with reduced shear strength and increased landslide susceptibility.

METHODOLOGY

The developed process, as represented in Figure 4, consists of five basic stages: (1) Searching for landslides using detailed field surveys and visual interpretation of Google Earth images; (2) Employing Frequency

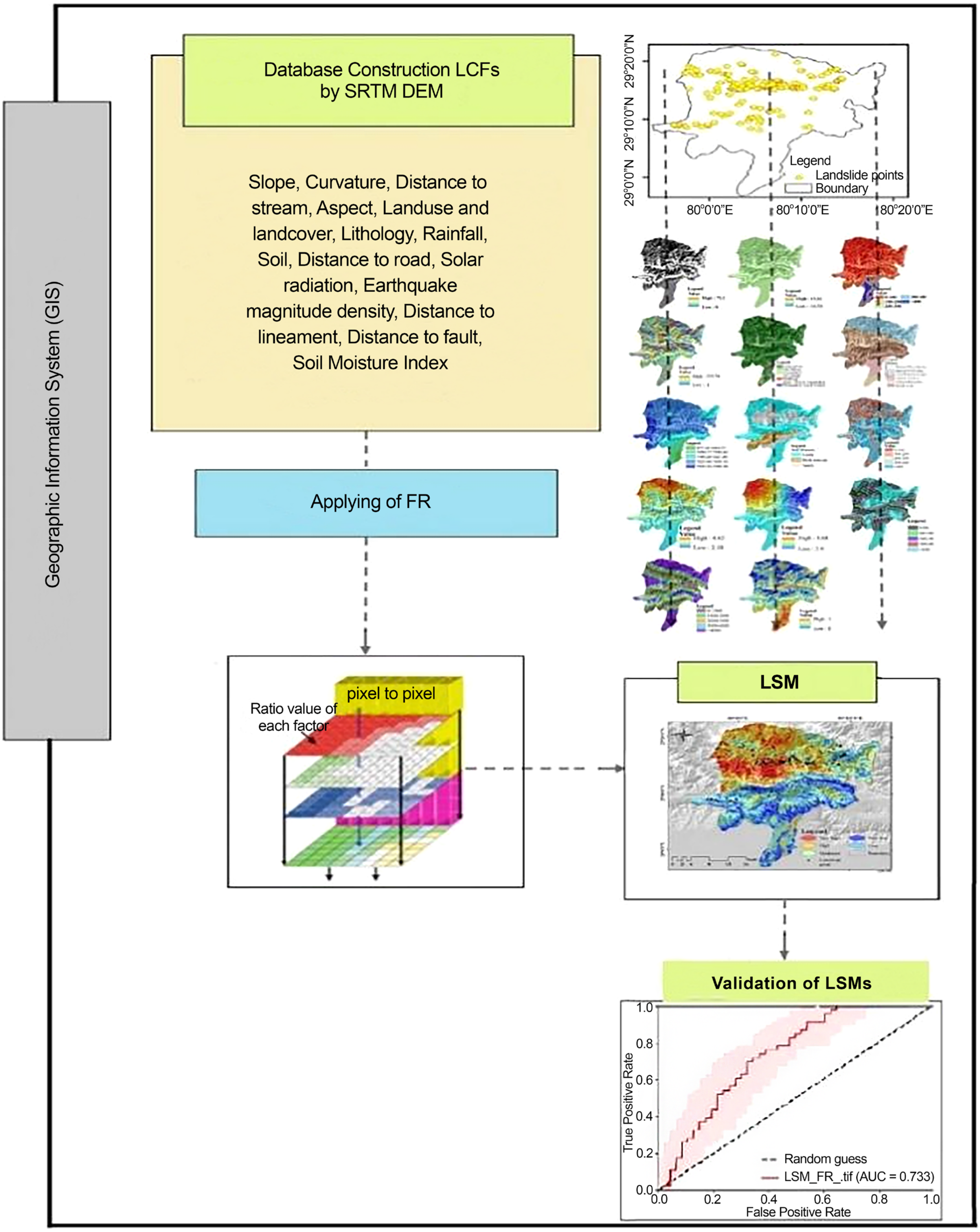

Fig. 4. Methodological flowchart (Source: Authors' own elaboration)

Ratio (FR) model to identify spatial relations between LCFs and landslide occurrence; (3) Comparison among LCF-based landslide models using statistical FR methods; and (4) Validation of LS models through AUC computation.

LANDSLIDE SUSCEPTIBILITY MODELS

Frequency Ratio (FR)

The frequency ratio (FR) technique is applied where the occurrence of landslides as well as spatial distribution of predictors are quantitatively associated. The quotient of each predictor class's percentage landslide area by the class's percentage of the total area represented is computed from this approach.

Formally, FR is calculated as:

$$FR = (X'/X) \,/\, (Y'/Y) = X''/Y'' \tag{1}$$

where:

- X' – the number of landslide pixels in every class predictor,
- X – the number of landslide pixels in the study area,
- Y' – the number of pixels for each predictor class,
- Y – the number of spectra in the region of interest,
- X'' – the fraction of the cumulative number of landslides in each predictor class,
- Y'' – the relative area of individual subclass in relation to the total area.

FR values are derived from these parameters, and they measure the predictor variable and landslides occurrence relationship. These parameters are then included into the framework of a GIS for the development of a landslide susceptibility index (Equation 2). The index assists in locating landslide-prone areas, considering the spatial distribution and importance of predictor variables in the area of interest.

$$LSI = \sum (FR)_i \; (i = 1, 2, \dots \dots, n) \tag{2}$$

where:

- LSI – the landslide susceptibility index,
- FR – the frequency ratio of each factor,
- n – the total number of input factors.

In this study, the Landslide Susceptibility Index (LSI) denotes the continuous pixel-wise index computed from the FR model, whereas the Landslide Susceptibility Map (LSM) refers to the classified LSI raster that is used for cartographic presentation and interpretation.

Prediction Rate (PR)

The contribution of each conditioning factor to landslide susceptibility was determined using the Prediction Rate (PR). A representative PR value for each conditioning factor was computed by aggregating its classes based on their individual Frequency Ratio (FR) values.

The PR values thus represent the total effect of each factor on landslide occurrence and subsequently used as weights during the Landslide Susceptibility Index (LSI) calculation as per Equation 3.

$$LSI = \sum\nolimits_{i=1}^{n} \left(P\,R_i \times F_i \right) \tag{3}$$

where:

- PR_i – the Prediction Rate weight associated with i-th conditioning factor,
- F_i – the corresponding thematic layer from reclassification, which was implemented in weighted overlay analysis.

Validation strategy

After developing the landslide susceptibility map for the Tanakpur block, it was important to validate the model's predictive performance. Internal validation was performed through comparison with the maps derived from FR model with the actual landslide inventory dataset through Receiver Operating Characteristics (ROC) method. The ROC analysis measures the model's performance of predicting landslide by comparing a probability image with a Boolean map of real occurrences. ROC curves illustrate the relationship between the true positive rate and the false positive rate, where a high performing model will have obtained an upper left corner position, which represents perfect predictions (Gorsevski et al., 2006). The AUC represents model predictive capability, which varies from 0.5 (random predictions) to 1.0 (perfect predictions) (Nandi and Shakoor, 2010). Higher AUC indicates better predictive capability essential for practical applications of landslide susceptibility models.

Results and discussion

Multicollinearity (Tolerance – TOL and Variance Inflation Factor – VIF) Test

The Tolerance (TOL) and the Variance Inflation Factor (VIF) were used to determine multi-collinearity among 14 conditioning factors. In these estimates, TOL values more than 0.1 and VIF value of less than 5 imply that the predictors are independent enough. Analysis of the variance provided TOL values above 0.9 and VIF near 1, indicating negligible multi--collinearity among other factors. This validates the selected conditioning factors, deeming them appropriate enough to be used in Fraction Ratio (FR) model (Table 2).

Result from FR Model

The Frequency Ratio (FR) values of all conditioning factor classes are provided in Table 3. Values of FR higher than 1 imply a positive correlation with landslide activator, while values lesser than one mean lower susceptibility. The Predictive Rate (PR) evaluates the overall contribution of every conditioning variable to landslides and was then applied as thematic weights while calculating final Landslide Susceptibility Index (LSI).

Spatial association of conditioning factors with landslide locations derived from the FR model

The FR analysis (Table 3) revealed distinct relationships between landslide occurrence and conditioning factors. Among topographic variables, slope gradient exhibited a strong impact on landslide occurrence, with the 45–60° class showing the highest FR value (4.69) despite occupying only 1.62% of the study area, thus indicating concentration of failures on steep terrain. Convex and concave curvature classes also showed slightly elevated FR values (1.07 and 1.03), suggesting that local surface geometry influences slope instability. Northeast- and west-facing slopes exhibited higher FR values (2.08 and 1.97), likely reflecting moisture-related microclimatic effects.

Hydrological factors were equally important. The strongest FR for stream proximity occurred at 0–100 m from drainage channels (FR = 1.34), corroborating the relationships identified between slope failure and both toe erosion and incision of streams into valley walls. Likewise, rainfall analysis indicated that the rainfall class of 1221.80–1303.32 mm/year had the greater FR (1.57) and encompassed 94.6% of all registered landslides, further demonstrating rain as one of main trigger agents.

Table 2. Multi-collinearity (TOL & VIF) analysis among the factors (Source: Authors' own elaboration)

Factors	R^2 Values	Tolerance (TOL) Values	Variance Inflation Factor (VIF) Values
Slope	0.071	0.929	1.076
Curvature	0.068	0.932	1.073
Stream	0.069	0.931	1.074
Aspect	0.068	0.932	1.073
LULC	0.068	0.932	1.073
Lithology	0.07	0.93	1.075
Rainfall	0.068	0.932	1.073
Soil	0.069	0.931	1.074
Distance to road	0.07	0.93	1.075
Solar radiation	0.069	0.931	1.074
Earthquake magnitude	0.065	0.935	1.069
Distance to lineament	0.065	0.935	1.069
Distance to fault	0.068	0.932	1.073
Soil moisture index	0.068	0.932	1.073

Table 3. FR model and the values with respect to fourteen conditioning factors (Source: Authors' own elaboration)

Factor	Class range	% Overall area (OA)	% Landslide area	FR	Prediction Rate (PR)
SLOPE	0–15	36.30	8.14	0.224205	4.0758
	15–30	42.28	42.8	1.013104	
	30–45	19.78	41.4	2.09251	
	45–60	1.62	7.58	4.691487	
	60–75	0.02	0.06	2.391491	
CURVATURE	CONVEX	45.43	48.9	1.07744	4.019925
	FLAT	4.25	0.59	0.138542	
	CONCAVE	50.32	50.5	1.002918	
STREAM	0–100	72.55	96.9	1.336226	8.268586
	100–200	15.37	3.06	0.199047	
	200–300	4.42	0	0	
	300–400	1.90	0	0	
	> 400	5.76	0	0	
ASPECT	–1	0.47	0	0	2.132399
	–22.5	5.77	5.53	0.958756	
	22.5–67.5	11.82	24.6	2.080038	
	67.5–112.5	13.73	11.5	0.839899	
	112.5–157.5	14.92	7.86	0.526871	
	157.5–202.5	15.21	6.06	0.398668	
	202.5–247.5	12.19	9.21	0.75524	
	247.5–292.5	10.66	21.2	1.986029	
	292.5–337.5	10.08	10.6	1.052485	
	337.5–360	5.16	3.45	0.669028	
LULC	Tree Cover	85.62	43.5	0.507773	7.450503
	Shrubland	0.10	0	0	
	Grassland	7.19	23.8	3.306184	
	Cropland	3.10	0.06	0.018089	
	Built-up	0.67	0.51	0.756232	
	Bare/Sparse Vegetation	1.92	32.2	16.75	
	Water bodies	1.40	0.03	0.019999	
LITHOLOGY	Bhaber and Tarai Alluvium	3.60	0	0	8.126604
	Piedmont fan Surface	9.32	0	0	
	Siwalik Group (Sub Himalaya)	32.63	88.1	2.700921	
	Klippen of Crystalline (Lesser Himalaya)	30.96	5.28	0.170417	
	Lower Paleozoic Granite (Lesser Himalaya)	0.44	0	0	
	Nagthat Formation (Lesser Himalaya)	23.05	6.6	0.286136	

Table 3. cont.

Factor	Class range	% Overall area (OA)	% Landslide area	FR	Prediction Rate (PR)
RAINFALL	977.252563-1058.76974	1.93	0	0	7.508983
	1058.76974-1140.286917	8.03	0.14	0.017473	
	1140.286917-1221.80409	19.31	2.44	0.126428	
	1221.804093-1303.32127	60.39	94.6	1.566572	
	1303.32127-1384.838446	10.34	2.81	0.271539	
SOIL	LOAM	60.48	90.7	1.500308	6.812435
	ROCK OUTCROP	10.97	1.46	0.133097	
	SANDY	28.56	7.8	0.273241	
DISTANCE TO ROAD	0–100	16.43	4.8	0.292116	3.626972
	100–200	12.28	4.18	0.34064	
	200–300	11.63	5.67	0.487675	
	300–400	8.48	5.44	0.642143	
	> 400	51.19	79.9	1.560957	
SOLAR RADIATION MAP	2.179-3.478733	5.34	56.9	10.64833	8.167508
	3.478733-3.727212	33.76	10.4	0.306797	
	3.727212-3.94702	29.03	26.1	0.900152	
	3.94702-4.214612	17.67	5	0.282748	
	4.214612-4.606443	14.20	1.63	0.114606	
EARTHQUAKE MAGNITUDE	2.9–3.254604	16.34	4.21	0.257627	4.738975
	3.254604–3.609208	42.73	55.7	1.304551	
	3.609208–3.963812	15.44	34.7	2.244303	
	3.963812–4.318415	10.57	3.68	0.347912	
	4.318415–4.673019	14.92	1.71	0.114751	
DISTANCE TO LINEAMENT	0–500	15.48	5.25	0.338982	2.27982
	500–1000	14.58	8.22	0.563983	
	1000–1500	13.56	20.1	1.479949	
	1500–2000	11.76	14.1	1.197739	
	> 2000	44.61	52.4	1.173893	
DISTANCE TO FAULT	0–1000	17.97	7.55	0.420168	2.839853
	1000–2000	16.04	9.99	0.622789	
	2000–3000	15.29	8.31	0.543324	
	3000–4000	14.42	26.5	1.836034	
	> 4000	36.28	47.7	1.314246	
SOIL MOISTURE INDEX	0–0.239216	15.77	20.6	1.304557	1
	0.239216–0.34902	29.78	23.9	0.802936	
	0.34902–0.454902	30.66	27.4	0.892644	
	0.454902–0.588235	17.27	19.1	1.108451	
	0.588235–1	6.52	9.01	1.380743	

Lithology strongly influenced susceptibility, with the Siwalik Group showing the highest FR value (2.70) and accounting for 88.1% of landslide pixels within the lithological classes, reflecting the weak and weathered nature of these formations. Similarly, loam soil exhibited elevated susceptibility (FR = 1.50), indicating the influence of soil properties on slope stability.

Land cover and anthropogenic factors also contributed to landslide occurrence. Grassland areas recorded the highest LULC-related FR value (3.31), whereas forested terrain showed comparatively lower susceptibility. Distance to road exhibited elevated FR in the > 400 m class (1.56), suggesting that naturally unstable remote terrain contributes substantially to landslide occurrence.

Among climatic and secondary triggering factors, low solar radiation zones showed the highest FR value (10.64), likely due to prolonged moisture retention, while moderate earthquake magnitude density classes exhibited positive association with landslide occurrence (FR = 1.30–2.24). Structural factors such as lineament and fault proximity also showed localized positive correlations, indicating the influence of fractured and tectonically weakened zones on slope instability.

Final Landslide Susceptibility map (LSM) was derived in GIS environment using equation 4 by means of FR-derived weights for all classes of conditioning factors. Finally, Landslide Susceptibility Index (LSI) was created, and classification of LSI into five classes was conducted (i.e. very low, low, moderate

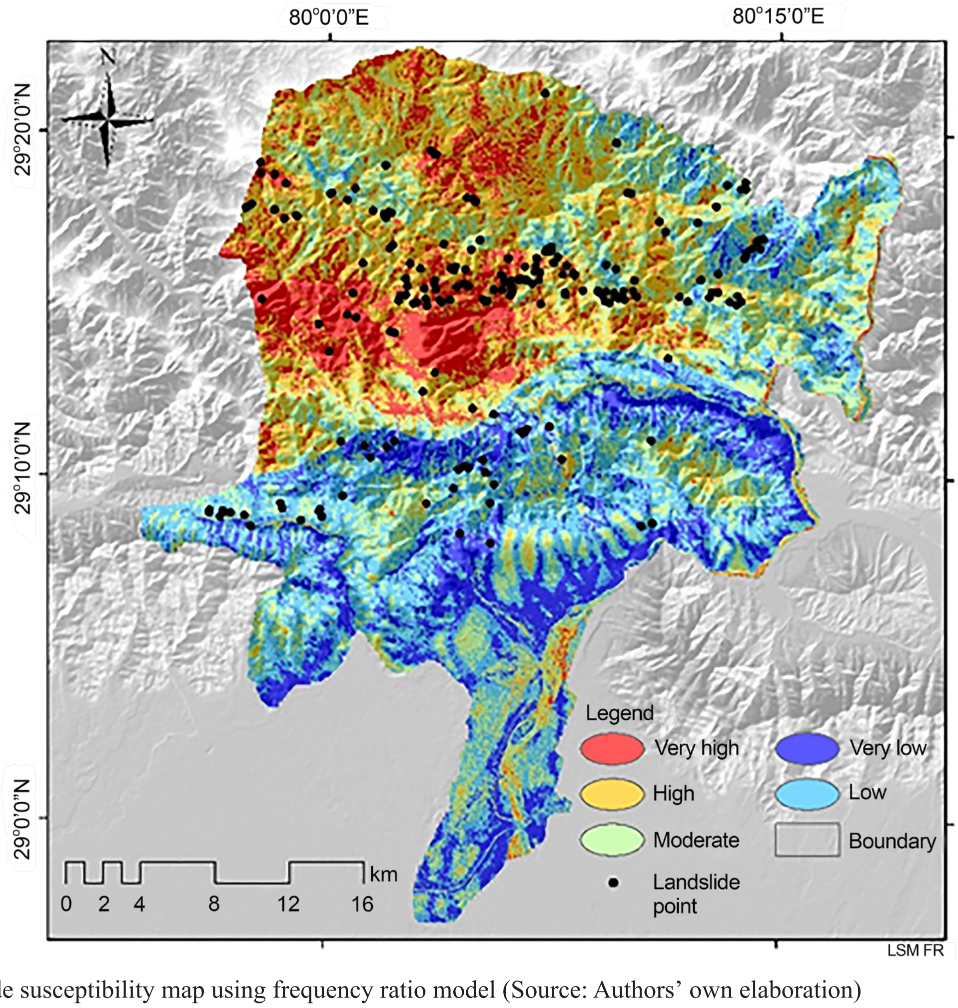

Fig. 5. Landslide susceptibility map using frequency ratio model (Source: Authors' own elaboration)

high and very high), using natural breaks (Jenks). The percentage share of the high and very high susceptibility zones in total study area is quite large, constituting 23.25% until reaching an expansive magnitude of a ratio equal to 11.46%.

$$LSM_{FR} = (WFR_{Slope}) + (WFR_{Curvature}) + (WFR_{aspect}) + \\ + (WFR_{LULC}) + (WFR_{Lithology}) + (WFR_{Rainfall}) + \\ + (WFR_{Soil}) + (WFR_{SolarRadiation}) + \\ +(WFR_{EarthMagnitudeDensity}) + (WFR_{SoilMoistureIndex}) + \\ + (WFR_{DistancetoFault}) + (WFR_{DistancetoStream}) + \\ + (WFR_{DistancetoRoad}) + (WFR_{DistancetoLineament}) \quad (4)$$

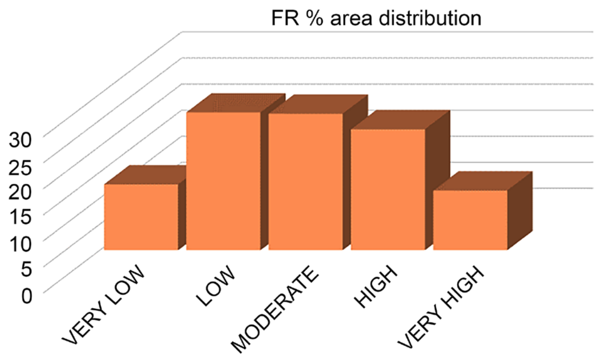

Fig. 6. Class distribution of the LSM_{FR} (Source: Authors' own elaboration)

Model validation

The landslide susceptibility model was statistically validated using Receiver Operating Characteristic (ROC) analysis and the Area Under Curve (AUC) formula. From this, 251 landslide locations were randomly divided into a training data set of 70% (175) and validation data set of 30% (76). The FR model had an AUC of 0.733 (73.3%) (Fig. 7), which meant the model was able to predict reliably and perform well in terms of distinguishing susceptible areas from non-susceptible ones.

DISCUSSION

The FR-based landslide susceptibility analysis of the Tanakpur Block (Table 2) demonstrated that slope instability is regulated through the combined influence of topographic, geological, hydrological, climatic, and human-related variables. Of these, slope gradient proved to be the most prominent variable having high FR at steep slopes (60–45°), further illustrating that terrain steepness is a major contributor in inducing gravitational instability. Similarly, formations of the Siwalik Group were more prone to failure due to their lithologic and weathering characteristics comprising weak interbedded sandstone and shale conglomerates, highly common in Sub-Himalayan regions.

Having said that, hydrological factors also play an important role, affecting landslides to a great extent. Places with 1221.80–1303.32 mm of annual precipitation and those within a distance margin of drainage channels under 100 m recorded the highest FR values. This indicates that pore water pressure from rainfall and toe erosion by flow are the principal triggering mechanisms. Furthermore, regions with lower levels of solar radiation were more susceptible as a consequence of the continued presence of moisture along with decreased rates for evapotranspiration.

Moreover, land cover also had an influence on slope stability: forest-covered areas tended to have lower susceptibility values, whereas grasslands and bare surfaces generally demonstrated higher FR. Proximity to lineaments and faults revealed local positive correlations, suggesting both tectonic disturbances and weakened rock mass conditions govern instability at other locations.

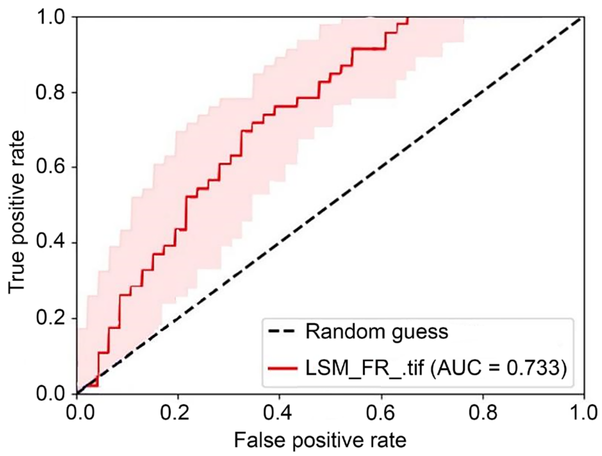

Fig. 7. Area under curve (AUC) values of FR model (Source: Authors' own elaboration)

The AUC obtained for the model (0.733) is in accordance with previous studies conducted in the Himalaya region, modelled using similar predictor variables and thresholding techniques (range 0.72–0.81). This validates the FR methodology, making it suitable for conducting regional-scale landslide susceptibility mapping in complex mountainous terrains.

The final susceptibility map indicates that 34.7% of the region is characterized as high to very high risk zones, requiring priority attention for hazard mitigation, slope stabilization, infrastructure planning, and land-use regulation. In particular, steep deforested slopes within Siwalik terrain and in close proximity to drainage channels should be prioritized for monitoring and bioengineering-based mitigation interventions.

CONCLUSION

To manage hilly terrain and lessen the impact produced by landslides, LSM is the first and most crucial step. Numerous quantitative and qualitative techniques for LSM have been established in recent years. Although no approach is currently thought to be clearly superior, each does have clear benefits and drawbacks alike. FR, which is statistically based methodology, was utilized in this work to address the drawbacks and highlight the benefits of LSM. In order to achieve this goal, an inventory dataset and 14 LCFs, namely: Slope, Curvature, Aspect, LULC, Lithology, Rainfall, Soil, Solar radiation intensity across terrain, Earthquake magnitude density, Soil moisture index, Distance to stream, roads, lineaments, and faults, respectively, were employed for the Landslide Susceptibility Mapping. The findings of FR demonstrated that the major factors influencing the incidence of landslides in the studied region were Drainage/stream density, Lithology, and Solar radiation intensity above ground. A number of other variables, including Soil, Rainfall, and LULC, show an active involvement in both causing and affecting landslides in the area. The validation findings demonstrated the superior performance and prediction accuracy of the FR model, with FR achieving 73.3%. The outcomes also demonstrated how the precision and caliber of the input parameters had a significant impact on the final LSM's prediction accuracy. According to the results of the framework that was introduced to the FR model, 23.27–23.67%, 11.47%, and 10.46% of the study region are situated in classes with high and extremely high vulnerability. This methodology's primary benefit is its capacity to ascertain the overall significance of causative factors and the spatial link among these elements and the sites where landslides occur. Human settlements and associated infrastructure are situated in places that are more susceptible to landslides; therefore, any building construction in these areas needs to be approached carefully and in accordance with engineering standards. The study's findings may be applied in sustainable development, landslip damage mitigation, and land-use management.

REFERENCES

Abedini, M., Tulabi, S. (2018). Assessing LNRF, FR, and AHP models in landslide susceptibility mapping index: a comparative study of Nojian watershed in Lorestan province, Iranian Journal of Earth Sciences, 77(11), 405. https://doi.org/10.1007/s12665-018-7524-1

Bisht, S., Rawat, K.S. (2024). Landslide Susceptibility Analysis Using GIS and Analytical Hierarchy Process (AHP) Approach for Disaster risk Reduction in the Mountainous Region: A Case Study of Lesser Himalayan Region. 2024 International Conference on Emerging Innovations and Advanced Computing (INNOCOMP). IEEE, Sonipat, India, 703–707. https://doi.org/10.1109/INNOCOMP63224.2024.00121

Bisht, S., Rawat, K.S., Singh, K.S. (2024). Earth observation data and GIS based landslide susceptibility analysis through frequency ratio model in lesser Himalayan region, India. Quaternary Science Advances, 13, 100141. https://doi.org/10.1016/j.qsa.2023.100141

Chouhan, S., Mukherjee, M. (2023). Design and application of a multi-hazard risk rapid assessment questionnaire for hill communities in the Indian Himalayan region. Natural Hazards and Earth System Sciences, 23, 1267–1286. https://doi.org/10.5194/nhess-23-1267-2023

Christen, M., Kowalski, J., Bartelt, P. (2010). RAMMS: Numerical simulation of dense snow avalanches in three-dimensional terrain. Cold Regions Science and Technology, 63, 1–14. https://doi.org/10.1016/j.coldregions.2010.04.005

Dubey, S., Sattar, A., Goyal, M.K., Allen, S., Frey, H., Haritashya, U.K., Huggel, C. (2023). Mass Movement Hazard and Exposure in the Himalaya. Earth's Future, 11, e2022EF003253. https://doi.org/10.1029/2022EF003253

Geological Survey of India (GSI). National Geoscience Data Repository (NGDR). https://geodataindia.gov.in/ (accessed: 14 July 2026).

Global Solar Atlas. Data Sources. https://globalsolaratlas.info/support/data-sources (accessed: 14 July 2026).

Google Earth Engine. https://earthengine.google.com/ (accessed: 14 July 2026).

Gorsevski, P.V., Gessler, P.E., Foltz, R.B., Elliot W.J. (2006). Spatial Prediction of Landslide Hazard Using Logistic Regression Model and ROC Analysis. Transactions in GIS, 10, 395–415. https://doi.org/10.1111/j.1467-9671.2006.01004.x

Huang, F., Cao, Z., Guo, J., Shui-Hua Jiang, S.-H., Li, S., Guo, Z. (2020). Comparisons of heuristic, general statistical and machine learning models for landslide susceptibility prediction and mapping. Catena, 191, 104580. https://doi.org/10.1016/j.catena.2020.104580

Jayangondaperumal, R., Thakur, V.C., Joevivek, V., Rao, P.S., Gupta, A.K. (2018). Active Tectonics of Kumaun and Garhwal Himalaya. Springer, Singapore.

Kirschbaum, D., Stanley, T., Zhou, Y. (2015). Spatial and temporal analysis of a global landslide catalog. Geomorphology, 249, 4–15. https://doi.org/10.1016/j.geomorph.2015.03.016

Mehta, A., Rawat, K.S. (2023). Monitoring flash flood using optical and microwave sensor dataset: A case study of Cachar district, Assam (India). Proceedings of the 2023 International Conference on Device Intelligence, Computing and Communication Technologies, (DICCT). IEEE, Dehradun, India, 90–94. https://doi.org/10.1109/DICCT56244.2023.10110185

Mergili, M., Fischer, J.T., Krenn, J., Pudasaini, S.P. (2017). r.avaflow v1, an advanced open-source computational framework for the propagation and interaction of two-phase mass flows. Geoscientific Model Development, 10(2), 553–569. https://doi.org/10.5194/gmd-10-553-2017

Nandi, A. Shakoor, A. (2010). A GIS-based landslide susceptibility evaluation using bivariate and multivariate statistical analyses. Engineering Geology, 110, 11–20. https://doi.org/10.1016/j.enggeo.2009.10.001

National Geoscience Data Repository (NGDR), Geological Survey of India (GSI) portal. https://geodataindia.gov.in/ (accessed: 14 July 2026).

National Remote Sensing Centre (NRSC), Indian Space Research Organisation (ISRO). Bhuvan Thematic Services. Available at: https://bhuvan-app1.nrsc.gov.in/thematic/thematic/index.php (accessed: 14 July 2026).

Rawat, K.S., Sahu, S.R., Singh, S.K. Mishra, A.K. (2022). Cloudburst analysis in the Nainital district. Himalayan Region, 2021. Discover Water 2(1), 12. https://doi.org/10.1007/s43832-022-00020-y

Rawat, K.S. Singh, S.K. (2023). Monitoring water spread and aquatic vegetation using earth observational data for Nani-High Altitude Lake (N-HAL) of Uttarakhand State, India. Journal of Engineering Research, 12, 64–74. https://doi.org/10.1016/j.jer.2023.10.014

Thakur, V.C. Rawat, B.S. (1992). Geological map of the Western Himalaya [Map]. Surveyor General of India.

Youssef, B., Bouskri, I., Brahim, B., Kader, S., Brahim, I., Abdelkrim, B., Spalević, V. (2023). The contribution of the frequency ratio model and the prediction rate for the analysis of landslide risk in the Tizi N'tichka area on the national road (RN9) linking Marrakech and Ouarzazate. Catena, 232, 107464. https://doi.org/10.1016/j.catena.2023.107464

HYBRYDOWE PODEJŚCIE WYKORZYSTUJĄCE MODEL WSPÓŁCZYNNIKA CZĘSTOTLIWOŚCI I TECHNOLOGIĘ GEOPRZESTRZENNĄ DO MAPOWANIA PODATNOŚCI NA OSUWISKA: STUDIUM PRZYPADKU

ABSTRAKT

Cel badania

Celem badania było wygenerowanie mapy podatności na osuwiska z wykorzystaniem hybrydowego podejścia modelu FR i technologii geoprzestrzennej dla badanego obszaru.

Materiały i metody

Zastosowano model FR i GIS.

Wyniki i wnioski

Według metody FR 11,5% badanego obszaru charakteryzuje się bardzo dużą podatnością na osuwiska, przy czym 23,2% to tereny o dużej podatności, a 26,2% to tereny o umiarkowanej podatności. Tereny o niskiej podatności stanowią 26,5%, a tereny o bardzo niskiej podatności na osuwiska – 12,6%. Klasy podatności na ostatecznie wygenerowanej mapie wyprowadzono z metody FR, pogrupowano według pięciu poziomów ryzyka i przeanalizowano za pomocą wartości pola pod krzywą (AUC, całka oznaczona). W odniesieniu do podziału obszarów objętych badaniem na strefy na podstawie wcześniejszych przypadków osuwisk, model FR wygenerował AUC na poziomie 73,4%. Zatem, wykorzystując ocenę mapy podatności na osuwiska, wykazano, że wyniki wygenerowane na podstawie zastosowanych metod charakteryzowały się zadowalającym stopniem wiarygodności.

Słowa kluczowe: współczynnik częstości, analityczny proces hierarchiczny, podatność na osuwiska, GIS, teledetekcja